MATERIALS AND METHODS

Materials The phospholipids, hydrogenated soybean phosphatidylcholine (HSPC) and (*N*-(carbonyl-methoxypolyethyleneglycol 2000)-1,2-distearoyl-*sn*-glycero-3-phosphoethanolamine (DSPE-PEG2000), were purchased from NOF Corporation (Tokyo, Japan). Cholesterol (Chol) was of analytical grade (Wako Pure Chemical Industries, Ltd., Osaka, Japan). Adriacin® injection 10 (Kyowa Hakko Kirin Co., Ltd., Tokyo, Japan), a doxorubicin hydrochloride (DXR) injection, was purchased from a general sales agency for drugs. The PD-10 desalting columns were purchased from GE Healthcare Japan (Tokyo, Japan). Centrifugal filter units, Amicon Ultra (10k MWCO), were purchased from MILLIPORE (Tokyo, Japan). HUVEC culture medium, HuMedia-EG2, which consisted of maintenance medium HuMedia-EB2, 2% Fetal Bovine Serum (FBS), 10 μg/L human epidermal growth factor, 5 mg/L human basic fibroblast growth factor, 10 mg/L heparin, 1 mg/L hydrocortisone, and antibiotics, was purchased from KURABO (Osaka, Japan). Dulbecco's modified Eagle's medium (DMEM) with high glucose and antibiotic cocktail were purchased from Invitrogen (Tokyo, Japan). Human serum (Biopredic International, Rennes, France) was obtained from KAC Co., Ltd. (Kyoto, Japan). Heparin sodium and carboxyfluorescein (CF) were reagent special grade (Wako Pure Chemical Industries, Ltd.).

Liposome Preparation Liposomes, liposome-encapsulated DXR, and liposome-encapsulated CF were prepared by the modified ethanol injection method.[17] DXR was encapsulated into liposomes by remote loading using an ammonium sulfate gradient.[18] Briefly, all lipids (200 μmol) were dissolved in about 5 mL of ethanol in different compositions: PEG-modified liposomes (sterically stabilized liposomes, SL), HSPC/Chol/DSPE-PEG2000 (55/40/5 mol/mol); normal liposomes (L), HSPC/Chol (6/4 mol/mol). The ethanol was removed with a rotary evaporator leaving behind about 1 mL of the ethanol solution. Next, 8 mL of 300 mM ammonium sulfate (for DXR-SL and DXR-L) or 100 mM CF dissolved in 10 mM Tris–HCl (pH 8.0) (for CF-SL and CF-L) was added to the ethanol solution. Liposomes formed spontaneously after further evaporation of the residual ethanol. Liposomes were then extruded through a series of polycarbonate filters (Nucleopore, Pleasanton, CA, U.S.A.) with pore sizes ranging from 0.4 to 0.1 μm. The mean diameter of extruded liposomes was in the range of 100–150 nm. Following extrusion, liposomes were ultracentrifuged at 80000 rpm for 45 min at 4°C, and suspended in normal saline or 10 mM Tris–HCl (pH 8.0) for liposome-entrapped DXR or CF respectively. Phospholipid concentration was determined by a colorimetric assay using Phospholipids C Test from Wako (Wako Pure Chemical Industries, Ltd.). For encapsulation of DXR, DXR was added to the ammonium sulfate-containing liposomes at a DXR/liposome ratio of 0.2 : 1 (w/w), and the liposomes were incubated for 1 h at 55°C. The liposome-encapsulated DXR and liposome-encapsulated CF were exchanged by eluting through a PD-10 desalting column equilibrated with normal saline.

Incubation of Liposome Liposomes were diluted with each test solution to a final lipid concentration of 0.2 mM in glass test tubes, and incubated at 37°C for 30 min in a water bath, without agitation. We observed that the aggregation of non-PEGylated liposomes with heparin occurred immediately. Thus, the intervals and temperature values were chosen to keep the experimental conditions constant. Only for photography, liposomes were incubated at 37°C for 6 h to observe significant precipitations. The final concentrations of ethylenediaminetetraacetic acid (EDTA) and heparin were 20 mM and 10 μg/mL respectively, unless otherwise indicated. The following solutions, 150 mM NaCl (saline), 150 mM KCl, 100 mM $CaCl_2$, 150 mM $MgSO_4$, 300 mM Glucose, and phosphate buffered saline (PBS) (pH 7.5) were prepared. Human serum was filtered by an ultrafiltration membrane before mixing with liposomes.

Zeta Potential Analysis Zeta potential was measured using an ELSZ-1000 (Otsuka Electronics Co., Ltd., Osaka, Japan), which is based on laser Doppler velocimetry in an electric field. CF-L, CF-SL, and negatively charged liposome (COATSOME EL-01-A, NOF Corporation) were diluted with saline to a final lipid concentration of 0.2–0.5 mM.

Particle Size Analysis The particle size distribution and mean diameter of each liposomal preparation after incubation was measured using a dynamic light scattering (DLS) photometer DLS-7000 (Otsuka Electronics Co., Ltd.) equipped with a He-Ne laser source (wavelength, 632.8 nm). All DLS measurements were made at a scattering angle of 90°. Data were gathered using a counting period of 100 s. Histogram analysis was performed to calculate the average particle size and standard deviation.

Binding and Uptake of Liposomes To assess the uptake or binding of liposomes by mononuclear phagocytes, we used a mouse macrophage cell line, RAW 264.7, which was kindly given by Dr. Tsunoda, Laboratory of Biopharmaceutical Research, National Institute of Biomedical Innovation. Cells were maintained in DMEM supplemented with 10% FBS and 1% antibiotic cocktail. Cells were seeded into 12-well plates (1×10^6 cells/well) and incubated at 37°C for 24 h. After incubation, aliquots of medium were removed, and cells were treated with CF-liposomes (0.2 mM) at 37°C for 1 h. The CF-liposomes were suspended in FBS- and antibiotic-free DMEM with the indicated concentration of $CaCl_2$ and 10 μg/mL heparin. After incubation, the cells were washed twice with ice-cold PBS and lysed by adding 500 μL of 0.5 M NaOH. Each lysate was diluted 4-fold with distilled water, and fluorescence of the CF in the lysate was measured at 490/520 nm (emission/excitation) using a spectrofluorometer (JASCO, Tokyo, Japan).

RESULTS AND DISCUSSION

The HUVEC culture medium, namely HuMedia EG-2, in which the aggregation of non-PEGylated liposomes had previously been observed in our study, is optimized for the maintenance and proliferation of normal cells. The HuMedia EG-2, which is composed of base medium HuMedia EB-2 and additives to enhance HUVEC proliferation, is a specialized culture medium. Among the additives in the medium (fetal bovine serum, antibiotics, heparin, hydrocortisone, human epidermal growth factor, human fibroblast growth factor), heparin was likely to interact with liposomes. Thus, DXR-L or DXR-SL was dispersed in base medium HuMedia EB-2, HuMedia EB-2 with heparin, and HuMedia EG-2, and we monitored the aggregation properties of these solutions. In the solution of DXR-L dispersed in base HuMedia EB-2, the aggregate was not observed, while significant aggregation occurred in

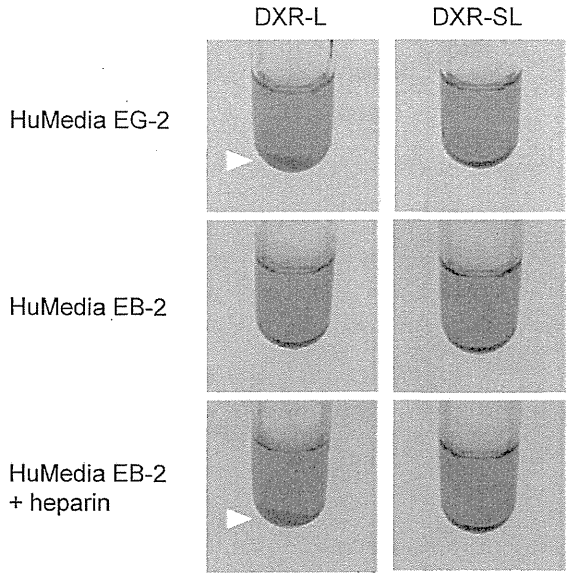

Fig. 1. Photographs of Liposomes (DXR-L and DXR-SL) Dispersed in HuMedia EG-2, HuMedia EB-2, or HuMedia EB-2 with Heparin

These photographs were taken after 6 h incubation at 37°C. An arrow indicates the precipitate of aggregates.

the solution of DXR-L dispersed in HuMedia EB-2 with heparin or HuMedia EG-2 (Fig. 1). There were no such changes in any of the solutions of the PEGylated liposome, DXR-SL. From these data, we concluded that the interaction of heparin with liposomes is responsible for the aggregation of DXR-L in HuMedia EG-2.

Next, to confirm whether heparin is the only cause of aggregation, DXR-L was dispersed in Eagle's minimum essential medium (MEM), which is commonly used for cell culture. There were no aggregates (data not shown). Heparin is a highly sulfated polymer that consists of a repeating disaccharide unit, including uronic acid and glucosamine, and is strongly negatively charged.[19] On the other hand, the non-PEGylated liposome DXR-L, mainly composed of phosphatidylcholine with a slightly negative charge, was quite unlikely to interact with heparin by itself to form aggregates. While the detailed composition of HuMedia EB-2 is proprietary, HuMedia EB-2 includes microelements (such as Zn, Cu, and Fe ions), which are not contained in common culture media, in addition to Ca^{2+} and Mg^{2+}. Thus, HuMedia EB-2 seems to be more similar to body fluids than other common culture media. Because of these factors, we hypothesized that bivalent ions are most likely to be involved in the interaction of non-PEGylated liposomes and heparin. We tested this hypothesis by adding the cation-chelating agent EDTA to the culture

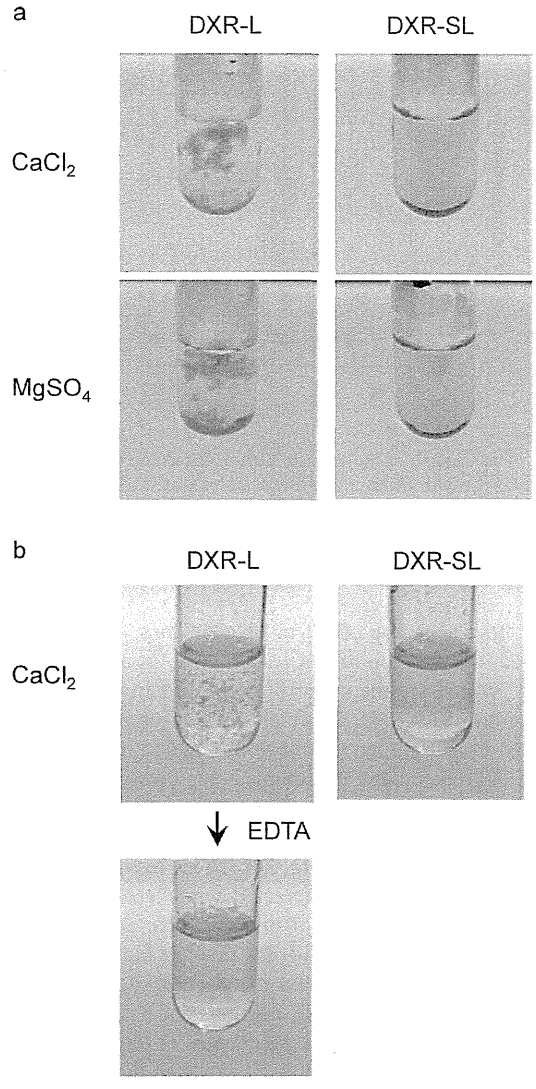

Fig. 2. Photographs of Liposomes (DXR-L and DXR-SL) Dispersed in $CaCl_2$ (100 mM) or $MgSO_4$ (150 mM) in the Presence of Heparin (10 μg/mL) (a)

Photograph of DXR-L dispersed in $CaCl_2$ (100 mM) in the presence of heparin (10 μg/mL) before and after the addition of EDTA, and that of DXR-SL as control (b).

medium, and then measured the particle size of DXR-L. We found that there were no changes in the particle size of DXR-L dispersed in the HuMedia EB-2 with heparin and EDTA, whereas the particle size of DXR-L in HuMedia EB-2 with heparin alone was increased to about 1000 nm (Table 1). These data suggest that bivalent ions are needed to form aggregates of liposomes with heparin.

Table 1. Effect of Ion for the Formation of Aggregation of DXR-L with Heparin in HUVEC Medium

	Particle size (nm)			
	HuMedia EG2	HuMedia EB2	HuMedia EB2 with heparin	HuMedia EB2 with heparin, EDTA
DXR-L	1266.7±49.6	142.8±0.6	942.4±90.2	144.3±1.3
DXR-SL	137.4±5.3	137.0±12.2	139.5±4.5	132.3±6.5

Each value represents the mean±S.D. (n=3). DXR-L and DXR-SL represent DXR encapsulated conventional liposome and PEGylated liposome, respectively.

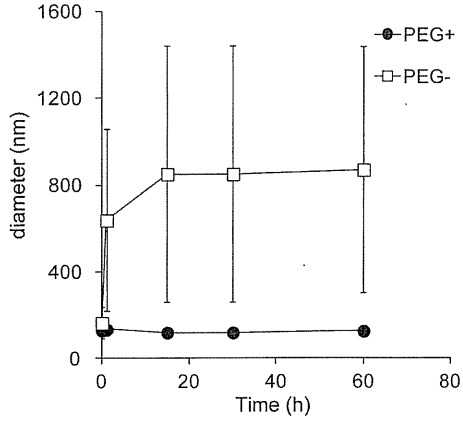

Fig. 3. The Change of the Particle Size of Liposomes (PEG +: CF-SL, PEG −: CF-L) with Time in the Presence of $CaCl_2$ (5 mM) and Heparin (10 μg/mL) at 37°C

Data represent the average particle size±S.D. (n=2) calculated by histogram analysis.

Next, to clarify the effect of bivalent ions, liposomes were dispersed in a solution of $CaCl_2$ or $MgSO_4$ as a source of Ca^{2+} or Mg^{2+}, which are the major bivalent ions in blood. Whereas the solution of DXR-SL in which the liposome was uniformly dispersed was red, the solution of DXR-L in which the liposome aggregated and precipitated was nearly clear (Fig. 2a). When EDTA was added after aggregation of DXR-L with heparin and Ca^{2+}, the formation of aggregation was reversed and the solution became clear (Fig. 2b). These results revealed that non-PEGylated liposome interacted with heparin and formed aggregates in the presence of bivalent ions, and the aggregations were reversible and did not involve the fusion of lipid membrane. Additionally, when the particle size of liposomes in other solutions (NaCl, KCl, glucose, and PBS) with heparin was measured, there were no aggregates of liposomes in these solutions (Table 2). This result emphasizes the importance of bivalent ions in driving the formation of liposomal aggregates with heparin.

In the above experiments, we used only one concentration of $CaCl_2$ (100 mM) or $MgSO_4$ (150 mM) solution. Thus, we assessed the dependence of the aggregation of liposome with heparin on Ca^{2+} and Mg^{2+} concentrations. To enable easy handling, we used carboxyfluorescein (CF)-encapsulated liposomes, namely CF-L or CF-SL, in this experiment. Firstly we investigated the time course of the formation of aggregation at 37°C. When CF-L was dispersed in the saline with heparin, its particle size was immediately increased (Fig. 3). Thus the samples were incubated for 30 min to keep the experimental conditions constant. The particle size of CF-L was significantly increased with increasing concentrations of Ca^{2+} and Mg^{2+} (Fig. 4). The increase of particle size was observed in

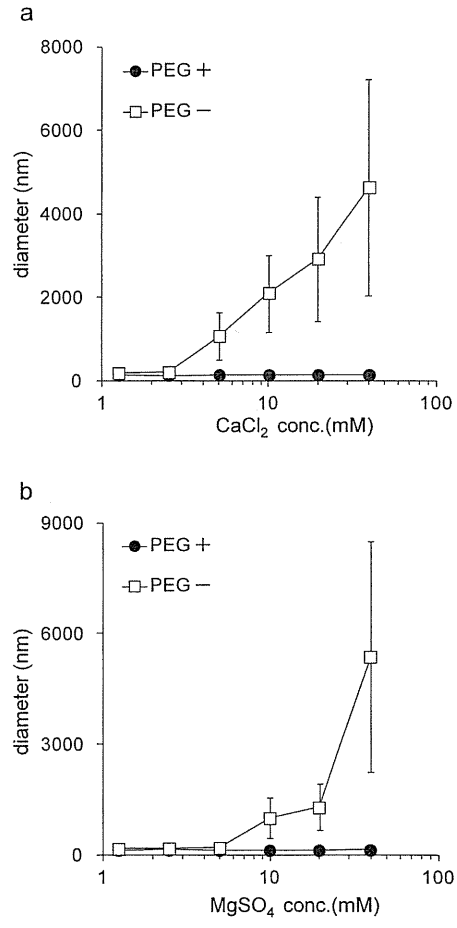

Fig. 4. The Effect of the $CaCl_2$ (a) or $MgSO_4$ (b) Concentration on the Particle Size of Liposomes (PEG +: CF-SL, PEG −: CF-L) in the Presence of Heparin (10 μg/mL)

Data represent the average particle size±S.D. (n=3) calculated by histogram analysis.

the presence of 2.5–5.0 mM Ca^{2+} or 5–10 mM Mg^{2+}. Because Ca^{2+} has a high affinity for heparin, Ca^{2+} could induce aggregation even at lower concentrations. Next, the effect of varying heparin concentrations on aggregation was assessed under a constant concentration (10 mM) of Ca^{2+} and Mg^{2+}. The particle size of CF-L was increased even at a low concentration of heparin (about 0.15 μg/mL) (Fig. 5). In the case of the PEGylated liposome CF-SL, no changes in the particle size were observed. It was possible that the surface charge prevent the aggregation of liposomes, because PEG-conjugated lipid (DSPE-PEG 2000) has negative charge. Thus, the surface charge of each liposome was measured (Table 3). As a result, non-PEGylated liposome CF-L and PEGylated liposome CF-SL exhibited a slightly negative surface charge, and there

Table 2. Particle Size of Liposome in Each Solution with Heparin

	Particle size (nm)					
	NaCl	KCl	$CaCl_2$	$MgSO_4$	Glucose	PBS
DXR-L	139.4±2.3	138.9±7.3	2830.0±137.8	4089.1±227.3	136.8±1.7	137.4±0.5
DXR-SL	128.3±8.8	132.3±0.4	129.8±0.5	141.3±1.8	137.9±3.0	131.9±8.3

Each value represents the mean±S.D. (n=3).

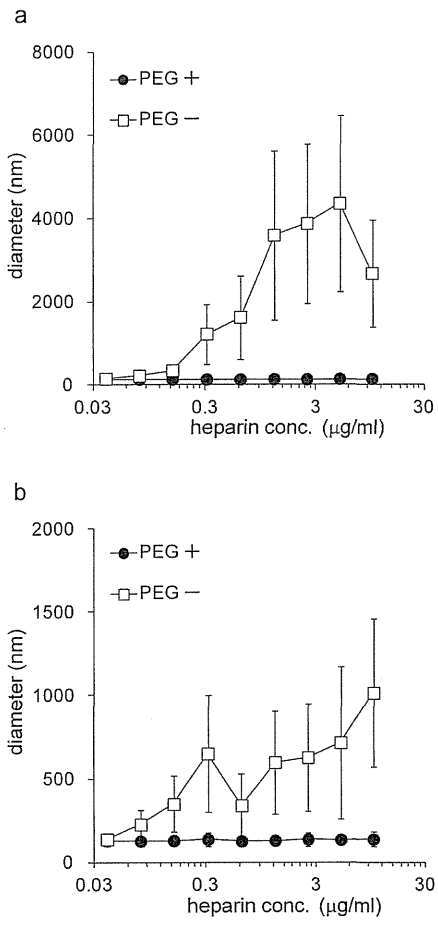

Fig. 5. The Effect of Varying Heparin Concentrations on the Particle Size of Liposomes (PEG +: CF-SL, PEG −: CF-L) in the Presence of $CaCl_2$ (10 mM) (a) or $MgSO_4$ (10 mM) (b)

Data represent the average particle size±S.D. (n=3) calculated by histogram analysis.

were no significant differences between CF-L and CF-SL in their zeta potential. Therefore, the prevention of aggregation could be due to a steric hindrance by PEG, which inhibits the interaction of the lipid membrane and heparin.

The aggregation induced by Ca^{2+} has been studied extensively in liposomes composed of negatively charged lipids.[20,21] It was also reported that, in liposomes composed of phosphatidylserine, Ca^{2+} induced aggregation, followed by membrane fusion.[22,23] The formation of aggregates observed in our study would not be accompanied by membrane fusion because the aggregate was reversible by the addition of EDTA. In the case of positively charged liposomes, formations of complexes with DNA and anionic polyions were also reported.[24,25] However, the aggregation of nearly neutral or slightly negatively-charged liposomes is poorly studied. Therefore, our results provide useful findings on the aggregation of such liposomes.

Table 3. Zeta Potential of Liposomes in Saline

Liposomes	Zeta-potential (mV)
CF-L	−3.46±0.72
CF-SL	−2.98±0.33
Anionic liposome	−44.29±1.29

Each value represents the mean±S.D. (n=2).

The normal levels of calcium and magnesium in serum are about 2.5 mM and 1.0 mM, respectively. In addition to calcium and magnesium, blood contains other positive ions, such as Fe, and Cu ions. The predicted lipid concentration after the administration of the liposomal product DOXIL® to human will be around 0.1 μmol/mL, which is close to the lipid concentration used in this study. Additionally the aggregation of non-PEGylated liposomes began at a concentration of Ca^{2+} between 2.5 and 5.0 mM in the above experiment. Therefore the possibility that the same phenomenon can occur *in vivo* cannot be eliminated. Next, to estimate the change in particle size of liposomes in blood circulation, the particle size of liposomes dispersed in ultrafiltered serum, which does not contain high molecular weight proteins, was measured. The particle size of DXR-L was significantly increased in the ultrafiltered serum with heparin, and the addition of EDTA inhibited the increase in particle size (Table 4). The particle size of the PEGylated liposome DXR-SL was slightly increased, and this was assumed to be caused by the interaction of DXR-SL with low molecular weight proteins or polypeptides in a multivalent ion-related fashion. This result suggested that slightly negatively-charged liposomes could possibly interact or aggregate with heparin in the blood circulation. However, when the same experiment was conducted using a different lot of serum, significant aggregation of DXR-L was not observed. More detailed examination is needed to demonstrate the aggregation of slightly negatively-charged liposomes in the blood circulation. In biological and human body conditions, in addition to heparin, there are other glycosaminoglycans, such as heparin sulfate and chondroitin sulfate. Therefore, the interaction of slightly negatively-charged liposomes with these anionic polymers also needs to be investigated in the future.

It has been assumed that the prolonged life-time of PEGylated liposomes is brought about by escape from the RES, whereas non-PEGylated liposomes are rapidly eliminated from blood circulation by phagocytes such as macrophages in the RES.[26] That is, whether the liposomes get trapped or evade the RES is an important feature that impinges on the *in vivo* behavior of liposomes. Therefore, we then assessed the effect of aggregate formation on the uptake of liposomes by macrophages. In this experiment, we used CF-L and CF-SL,

Table 4. Particle Size of Liposomes in Ultrafiltrated-Serum

	Particle size (nm)			
	None	With EDTA	With heparin	With heparin, EDTA
DXR-L	401.0±17.8	127.6±3.9	2201.1±56.8	136.1±2.2
DXR-SL	174.5±10.2	131.3±1.5	165.0±9.6	142.3±1.4

Each value represents the mean±S.D. (n=3).

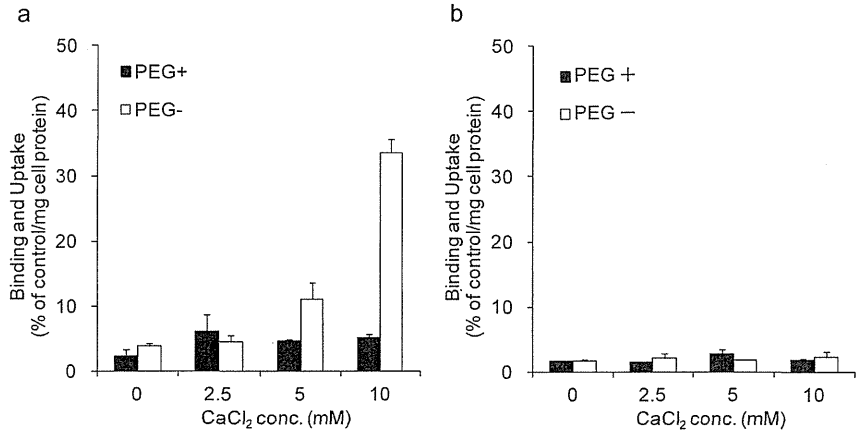

Fig. 6. Uptake and Binding Rate of Liposomes (PEG +: CF-SL, PEG −: CF-L) by Macrophages in the Presence of Ca^{2+} and Heparin (a) or in the Absent of Heparin (b)

Liposomes, dispersed in DMEM with $CaCl_2$ at the indicated concentration in the presence or the absent of heparin (10 μg/mL), were incubated for 30 m at 37°C, and added to cells. After incubating for 1 h at 37°C, the cells were washed, lysed with 0.5 M NaOH, and the concentration of the CF in cells was calculated. Each value represents the mean±S.D. of 3 replicates.

and murine RAW 264.7 cells as the test macrophage cell line. We measured the binding and uptake of these liposomes by RAW 264.7 cells at the indicated concentration of Ca^{2+} in the presence of 10 μg/mL heparin. The binding and uptake rates of CF-L were increased with increasing concentrations of Ca^{2+}, whereas in the case of the PEG-liposome CF-SL, the binding and uptake rates were not increased (Fig. 6). Therefore, these data revealed that the binding and uptake rates of CF-L were increased upon increasing the aggregation of CF-L with heparin/Ca^{2+}. This increased binding and uptake is likely caused by the tendency of phagocytes, such as macrophages, to take up larger particles more readily.[27] Additionally, scavenger receptors, whose ligands are anionic macromolecules as well as degenerated-LDL, are expressed on the cell surface of macrophages, and are involved in the phagocytosis of foreign substances and waste products.[28] Therefore, the increase in uptake rate with increasing particle size could be affected by the strong negative charge of the heparin contained in the aggregate. On the other hand, the uptake of CF-SL was not changed, because CF-SL did not interact with heparin and its particle size remained small even at a high concentration of Ca^{2+}.

Our data indicate that slightly negatively-charged liposomes aggregate with heparin in the presence of bivalent ions such as Ca^{2+} and Mg^{2+}. Our data also indicate that the interaction of such liposomes with heparin can be prevented by modification with PEG. The measurement of particle size by DLS revealed the quantitative relationship between Ca^{2+}/Mg^{2+} (or heparin) and the formation of aggregates. Additionally, we measured the binding and uptake of liposomes by macrophages, and found that the heparin-mediated aggregation of liposomes can enhance the binding and uptake of liposomes.

Acknowledgements We thank Professor Maitani, Hoshi University, and Professor Mruyama and Dr. Suzuki, Teikyo University, for their advice regarding the preparation of stealth liposomes. This study was supported by the Research on Publicly Essential Drugs and Medical Devices from the Japan Health Sciences Foundation (KHB1005).

REFERENCES

1) Allen TM, Hansen C, Martin F, Redemann C, Yau-Young A. Liposomes containing synthetic lipid derivatives of poly(ethylene glycol) show prolonged circulation half-lives *in vivo*. *Biochim. Biophys. Acta*, **1066**, 29–36 (1991).
2) Klibanov AL, Maruyama K, Torchilin VP, Huang L. Amphipathic polyethyleneglycols effectively prolong the circulation time of liposomes. *FEBS Lett.*, **268**, 235–237 (1990).
3) Papahadjopoulos D, Allen TM, Gabizon A, Mayhew E, Matthay K, Huang SK, Lee KD, Woodle MC, Lasic DD, Redemann C. Sterically stabilized liposomes: improvements in pharmacokinetics and antitumor therapeutic efficacy. *Proc. Natl. Acad. Sci. U.S.A.*, **88**, 11460–11464 (1991).
4) Mori A, Klibanov AL, Torchilin VP, Huang L. Influence of the steric barrier activity of amphipathic poly(ethylene glycol) and ganglioside GM1 on the circulation time of liposomes and on the target binding of immunoliposomes *in vivo*. *FEBS Lett.*, **284**, 263–266 (1991).
5) Du H, Chandaroy P, Hui SW. Grafted poly(ethylene glycol) on lipid surfaces inhibits protein adsorption and cell adhesion. *Biochim. Biophys. Acta*, **1326**, 236–248 (1997).
6) Senior J, Delgado C, Fisher D, Tilcock C, Gregoriadis G. Influence of surface hydrophilicity of liposomes on their interaction with plasma protein and clearance from the circulation: studies with poly(ethylene glycol)-coated vesicles. *Biochim. Biophys. Acta*, **1062**, 77–82 (1991).
7) Allen TM, Austin GA, Chonn A, Lin L, Lee KC. Uptake of liposomes by cultured mouse bone marrow macrophages: influence of liposome composition and size. *Biochim. Biophys. Acta*, **1061**, 56–64 (1991).
8) Chiu GN, Bally MB, Mayer LD. Selective protein interactions with phosphatidylserine containing liposomes alter the steric stabilization properties of poly(ethylene glycol). *Biochim. Biophys. Acta*, **1510**, 56–69 (2001).
9) Xu Z, Marchant RE. Adsorption of plasma proteins on polyethylene oxide-modified lipid bilayers studied by total internal reflection fluorescence. *Biomaterials*, **21**, 1075–1083 (2000).
10) Dos Santos N, Allen C, Doppen AM, Anantha M, Cox KA, Gallagher RC, Karlsson G, Edwards K, Kenner G, Samuels L, Webb MS, Bally MB. Influence of poly(ethylene glycol) grafting density and polymer length on liposomes: relating plasma circulation lifetimes to protein binding. *Biochim. Biophys. Acta*, **1768**, 1367–1377 (2007).

11) Price ME, Cornelius RM, Brash JL. Protein adsorption to polyethylene glycol modified liposomes from fibrinogen solution and from plasma. *Biochim. Biophys. Acta*, **1512**, 191–205 (2001).
12) Burgess DJ, Hussain AS, Ingallinera TS, Chen ML. Assuring quality and performance of sustained and controlled release parenterals: AAPS workshop report, co-sponsored by FDA and USP. *Pharm. Res.*, **19**, 1761–1768 (2002).
13) Shibata H, Saito H, Yomota C, Kawanishi T. Ammonium ion level in serum affects doxorubicin release from liposomes. *Pharmazie*, **65**, 251–253 (2010).
14) Shibata H, Kawanishi T, Yomota C. Basic Examination for *in Vitro* Release Test of Drug-Encapsulated Liposome, *PSWC/AAPS Annual Meeting and Exposition*, M1345 (2010)
15) Senior J, Crawley JC, Gregoriadis G. Tissue distribution of liposomes exhibiting long half-lives in the circulation after intravenous injection. *Biochim. Biophys. Acta*, **839**, 1–8 (1985).
16) Senior JH. Fate and behavior of liposomes *in vivo*: a review of controlling factors. *Crit. Rev. Ther. Drug Carrier Syst.*, **3**, 123–193 (1987).
17) Maitani Y, Soeda H, Junping W, Takayama K. Modified ethanol injection method for liposomes containing β-sitosterol β-D-glucoside. *J. Liposome Res.*, **11**, 115–125 (2001).
18) Haran G, Cohen R, Bar LK, Barenholz Y. Transmembrane ammonium sulfate gradients in liposomes produce efficient and stable entrapment of amphipathic weak bases. *Biochim. Biophys. Acta*, **1151**, 201–215 (1993).
19) Mulloy B, Forster MJ. Conformation and dynamics of heparin and heparan sulfate. *Glycobiology*, **10**, 1147–1156 (2000).
20) Lansman J, Haynes DH. Kinetics of a Ca^{21}-triggered membrane aggregation reaction of phospholipid membranes. *Biochim. Biophys. Acta*, **394**, 335–347 (1975).
21) Chauhan A, Chauhan VP, Brockerhoff H. Effect of cholesterol on Ca^{2+}-induced aggregation of liposomes and calcium diphosphatidate membrane traversal. *Biochemistry*, **25**, 1569–1573 (1986).
22) Morris SJ, Gibson CC, Smith PD, Greif PC, Stirk CW, Bradley D, Haynes DH, Blumenthal R. Rapid kinetics of Ca^{2+}-induced fusion of phosphatidylserine/phosphatidylethanolamine vesicles. The effect of bilayer curvature on leakage. *J. Biol. Chem.*, **260**, 4122–4127 (1985).
23) Wilschut J, Düzgüneş N, Fraley R, Papahadjopoulos D. Studies on the mechanism of membrane fusion: kinetics of calcium ion induced fusion of phosphatidylserine vesicles followed by a new assay for mixing of aqueous vesicle contents. *Biochemistry*, **19**, 6011–6021 (1980).
24) Bordi F, Cametti C, Sennato S, Diociaiuti M. Direct evidence of multicompartment aggregates in polyelectrolyte-charged liposome complexes. *Biophys. J.*, **91**, 1513–1520 (2006).
25) Cametti C. Polyion-induced aggregation of oppositely charged liposomes and charged colloidal particles: the many facets of complex formation in low-density colloidal systems. *Chem. Phys. Lipids*, **155**, 63–73 (2008).
26) Lasic DD, Martin FJ, Gabizon A, Huang SK, Papahadjopoulos D. Sterically stabilized liposomes: a hypothesis on the molecular origin of the extended circulation times. *Biochim. Biophys. Acta*, **1070**, 187–192 (1991).
27) Chono S, Tauchi Y, Morimoto K. Pharmacokinetic analysis of the uptake of liposomes by macrophages and foam cells *in vitro* and their distribution to atherosclerotic lesions in mice. *Drug Metab. Pharmacokinet.*, **21**, 37–44 (2006).
28) Kodama T, Freeman M, Rohrer L, Zabrecky J, Matsudaira P, Krieger M. Type I macrophage scavenger receptor contains α-helical and collagen-like coiled coils. *Nature*, **343**, 531–535 (1990).

J Pharm Innov (2012) 7:87–93
DOI 10.1007/s12247-012-9130-1

RESEARCH ARTICLE

Coating and Density Distribution Analysis of Commercial Ciprofloxacin Hydrochloride Monohydrate Tablets by Terahertz Pulsed Spectroscopy and Imaging

Tomoaki Sakamoto · Alessia Portieri · Donald D. Arnone · Philip F. Taday · Toru Kawanishi · Yukio Hiyama

Published online: 25 May 2012

Abstract Terahertz pulsed spectroscopy was used to qualitatively detect ciprofloxacin hydrochloride monohydrate (CPFX·HCl·H_2O) in tablets, and terahertz pulsed imaging (TPI) was used to scrutinize not only the coating state but also the density distribution of tablets produced by several manufacturers. TPI was also used to evaluate distinguishability among these tablets. The same waveform, which is a unique terahertz absorption spectrum derived from pure CPFX·HCl·H_2O, was observed in all of the crushed tablets and in pure CPFX·HCl·H_2O. TPI can provide information about the physical states of coated tablets. Information about the uniformity of parameters such as a coating thickness and density can be obtained. In this study, the authors investigated the coating thickness distributions of film-coated CPFX·HCl·H_2O from four different manufacturers. Unique terahertz images of the density distributions in these commercial tablets were obtained. Moreover, B-scan (depth) images show the status of the coating layer in each tablet and the density map inside the tablets. These features would reflect differences resulting from different tablet-manufacturing processes.

Keywords Terahertz pulsed spectroscopy · Terahertz pulsed imaging · Coating · Density distribution · Tablet · Imaging methods · Ciprofloxacin

T. Sakamoto (✉) · T. Kawanishi · Y. Hiyama
Division of Drugs, National Institute of Health Sciences, Tokyo 158-8501, Japan
e-mail: tsakamot@nihs.go.jp

A. Portieri · D. D. Arnone · P. F. Taday
TeraView Ltd., Cambridge CB4 0WS, UK

Introduction

The electro-magnetic wave on terahertz region is generally defined from 0.1 THz to 10 THz (3.3 to 333 cm^{-1}). This electro-magnetic region has also been known as a far-infrared wave region. But, an irradiated light energy from a typical far-infrared spectrometer equipped with a high-pressure mercury lamp will drop at a frequency below 1 THz drastically. Recent development of laser devices and semi-conductors has allowed us to use coherent terahertz wave with lower frequency. In a terahertz region, vibrational information about weak intermolecular energy such as crystal lattice, hydrogen bonding, and van der Waals force can be detected [1–6]. This leads to applications in the pharmaceutical and chemical industries such as the detection of polymorphs [2, 7–13]. A number of authors have shown that unique terahertz spectra can be obtained for active pharmaceutical ingredients (APIs), illegal drugs, and explosives [7, 9, 12]. The assignment of spectroscopic bands in this region of the spectrum remain challenging due to the complicated properties of crystalline materials, but a number of groups are having some success. Comparative studies between hydrates and their anhydrides have been reported by Kogermann et al. [14] and others [15, 16]. These authors have also investigated the thermodynamics of phase transformation following dehydration.

A time domain terahertz technology (terahertz pulsed technology) is non-destructive analytical tool for investigating pharmaceutical materials and products. This technique can provide two modes which are an imaging mode known as terahertz pulsed imaging (TPI) and a spectroscopic mode known as terahertz pulsed spectroscopy (TPS). Especially, TPI can produce images or maps which are obtained by detecting reflected pulses from each pixel on a tablet or

other dosage forms. Terahertz pulses are irradiated at each pixel on a tablet and penetrate, and echoes or reflections from layers are measured. Then, TPI also obtain depth information at each pixel. The detection time and intensity of reflected wave is affected by the refractive index of the sample. For a coated tablet, this time-of-flight technique makes detector distinguish different arriving time of terahertz pulse. The reflected pulses which are originated from the interface between coating layer and the surface of core tablet or another coating layer in the tablet are detected, and information of the time of flight is used not only to calculate the coating thickness but also to acquire 3D images of a coated tablet. Ho et al. [17–19] reported that not only the coating thickness but also the density of the coating can influence the quality performance of sustained-release film-coated tablets. The authors were able to use the intensity of the terahertz reflected pulse from a coating to model the changes in refraction of terahertz pulsed wave which is correlated with changes in density of coating [19–21]. Recently, we applied TPI to the nondestructive testing of a transdermal drug delivery system. These products have a crystal reservoir system inside a membrane that controls the release rate of an active ingredient from the matrix into the skin by forming crystals [22]. Thus, a terahertz pulse wave can penetrate comparatively deeply and provide physical and/or chemical information inside a solid pharmaceutical nondestructively. These advantages suggest that TPI would be applicable as a nondestructive analytical tool not only for process control but also for the quality analysis of commercial products.

In this paper, we compare the terahertz absorption spectra of pure API component with those contained within the solid dosage form. We also obtain terahertz images of four film-coated ciprofloxacin hydrochloride monohydrate ($CPFX{\cdot}HCl{\cdot}H_2O$) tablets. In this product, the coating has the very important role of protecting the API against degradation caused by light and/or humidity. The authors analyze the coating uniformity and the density of components inside tablets and evaluate the distinguishability among several kinds of commercial tablets that have the same clinical application.

Experimental

Materials

To obtain the terahertz absorption spectra of pure materials, $CPFX{\cdot}HCl{\cdot}H_2O$ was purchased from Wako Pure Chemical Industries Ltd. (Osaka, Japan). This compound was used without any further purification. Polyethylene (particle size,<80 μm) used to prepare the sample pellets was purchased from Induchem AG (Volketswil, Switzerland).

$CPFX{\cdot}HCl{\cdot}H_2O$ tablets were obtained from five different commercial sources (Bayer Healthcare Co. Ltd. (Osaka, Japan), Sawai Pharmaceutical Co. Ltd. (Osaka, Japan), Nichi-iko Pharmaceutical Co. Ltd. (Toyama, Japan), Choseido Pharmaceutical Co. Ltd. (Tokushima, Japan) and J-Dolph Pharmaceutical Co. Ltd. (Shiga, Japan)).

All commercial tablets used in this study were a round shape and had a central band. The weight, diameter, and labeled amount were 305 to 310 mg, about 10 mm, and 232.8 mg (as hydrochloride salt monohydrate), respectively.

Instruments and Measurement Conditions

The terahertz pulsed spectra of the pure $CPFX{\cdot}HCl{\cdot}H_2O$ and the crushed commercial tablets were obtained using TPS Spectra 3000 terahertz spectrometer (TeraView Ltd., Cambridge, UK). Each sample was measured using a spectral range from 120 to 2 cm^{-1} and a spectral resolution of 1.5 cm^{-1}. A spectrum was obtained by averaging 1,800 scans and took 1 min. Measurements were obtained by transmittance mode in a dry nitrogen-purged sample compartment. Blackman–Harris term 3 was used as the apodization function. The data were collected using TPS spectra version 1.17.0 (TeraView Ltd.).

Discs were prepared by mixing the pure sample with polyethylene powder at a 10 % (*w/w*) concentration, and the two components were mixed well. Then, 400 mg of the mixture was pressed at 2 tons for 2 min to form a disc between 3 and 4 mm thick and with a diameter of 13 mm.

Whole tablets were crushed in a mortar. A portion of the powder equivalent to 10 % API was put into another mortar, up to 200 mg polyethylene powder was added per pellet, and the two were mixed together well. Then a pellet was prepared in the same manner as described above.

Terahertz images of tablets were obtained using the TPI imaga 2000 Coating Scan system (TeraView Ltd.). The operation of this system was well described by Zeitler et al. [11]. Images were acquired in a point-to-point mode with a step size of 100 μm. Three measurements of each tablet were taken, and the measurements together took about 30 min/tablet. Images were analyzed using TPI View version 2.3.10. No sample preparation was required.

Results and Discussion

Identification of $CPFX{\cdot}HCl{\cdot}H_2O$ in Tablets Using TPS

The terahertz absorption spectra of the crushed tablets are shown in Fig. 1. Tablets A, B, C, and D show similar spectral features while tablet E exhibits a different spectrum (especially lower wavenumber than 40 cm^{-1}). By comparing these spectra to the pure chemical species, we can see

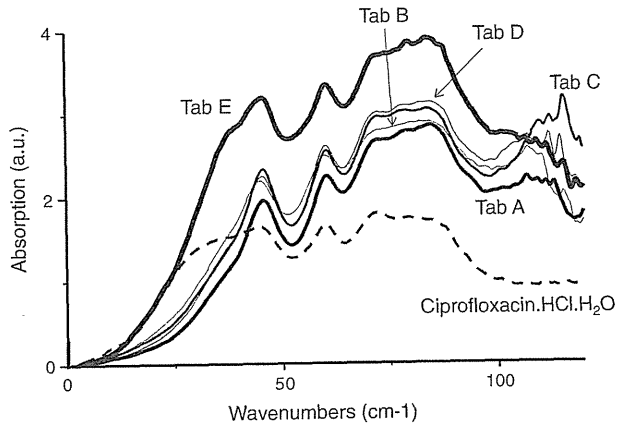

Fig. 1 Terahertz spectra of ciprofloxacin hydrochloride monohydrate (*broken line*) and five different commercial tablets (*solid lines*)

that tablets A, B, C, and D are all consistent with each other and with the spectra of CPFX·HCl·H_2O (broken line). Although the spectral feature of tablet E was different from those of the other tablets, the spectral feature that is lower wavenumber than 40 cm^{-1} was similar to that of CPFX·HCl·H_2O. According to the enclosed documents for the products, CPFX·HCl·H_2O is the active ingredient in each product. These results suggest that terahertz spectroscopy can be used to identify API in tablets.

Figure 2 shows the second derivative of terahertz absorption spectra obtained from the commercial tablets. The peaks at 60 and 46 cm^{-1} were observed in all of the tablets. The peaks at 88, 85, 84, 79, and 71 cm^{-1} detected in tablet A may be water vapor lines.

Table 1 shows the ingredients listed in the manufacturer's product literature. This shows that similar ingredients are used for all tablet formulations. Unfortunately, the literature does not disclose the percentage content of each ingredient.

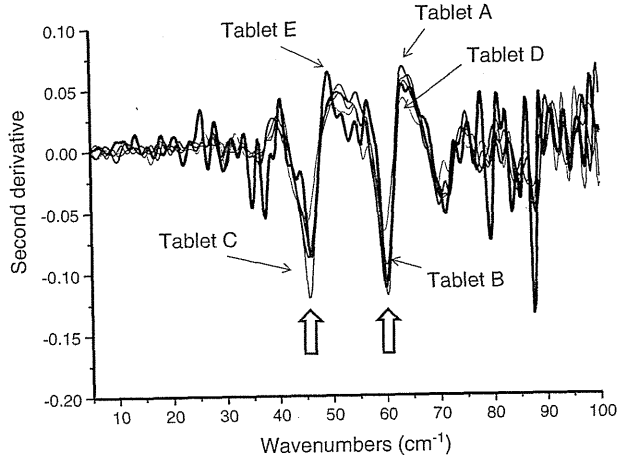

Fig. 2 Second derivative terahertz spectra of the five different commercial tablets

Analysis of Quality Attributes of Tablets Using Terahertz Imaging System

Density Distribution of Film-Coated Tablets

Figure 3 shows the distribution maps of the reflected peak intensities from the surface (A) and 0.26 mm depth (B) of the tablets obtained from each of the measured commercial tablets, respectively. Tablets A and B each have a homogeneous distribution of the peak reflected strength from the surface of the coating, while tablets C and D each have a heterogeneous distribution. As discussed previously, Ho et al. [17] correlated the intensity of reflection to the refractive index of the coating from the equation

$$R = \frac{(n-1)}{(n+1)}$$

where R is the intensity of the reflection and n is the terahertz refractive index of the material. The intensity of reflection from each tablet measured is shown in Fig. 3; these values are labeled with the letter A. They indicate differences between each of the tablets. From the equation described above, we can relate the R to the terahertz refractive index of the coating. This is an indication of a change in the density of the coating. During scale-up of a sustained-release coating product, Ho et al. [19] also showed that similar changes in the density of the coating (or in the intensity of reflection from the tablet) can affect product performance. In the case of the tablets studied in this paper, the coating prevents the decomposition of API by light exposure. So, we do not expect the coating to affect the tablets' dissolution performance. However, this study will provide the sensitivity needed for terahertz measurements against this parameter. We also observe a variation in the intensity of reflection across the surfaces of tablets A and B. This may suggest regions of defective coating or changes in local density on the tablets.

A terahertz dataset allows the experimenter to generate maps at different depths within a tablet without sectioning the tablet. Image B in Fig. 3 shows the distribution of relative refractive indices changing from the tablet surface to a depth of 260 μm. In the images of tablets A and D, the changes in refraction of terahertz pulsed wave by penetrating of component which has different refractive indices are larger at the centers of the tablets than at their outer circles. And tablet B shows comparatively large changes in refraction of terahertz pulsed wave through the wider area of the tablet. In the image obtained from tablet C, small areas having comparatively small changes in refraction of terahertz pulsed wave appear in the center of the tablet. Meanwhile, the edge of the tablet shows larger change in

Table 1 Ingredients contained in each of five commercial tablets

Tablet A		
Corn starch	Magnesium stearate	Cellulose
Titanium dioxide	Hydroxypropylmethylcellulose (HPMC)	
Carboxymethylstarch soduim	Povidon	Silicate unhydrate
Tablet B		
Corn starch	Cellulose	Magnesium stearate
Titanium dioxide	HPMC	
Macrogol	Crosspovidon	Silicate unhydrate
Tablet C		
Corn starch	Crystallized cellulose	Magnesium stearate
Titanium dioxide	HPMC	
Macrogol 6000	Light anhydrous silicic acid	Tarc
Carboxymethylstarch soduim	Lactose	Carnauba wax
Tablet D		
Corn starch	Hydroxypropylcellulose	Magnesium stearate
Titanium dioxide	HPMC	
Macrogol	Carboxymethylstarch sodium	Citric acid hydrate
Tablet E		
Corn starch	Crystallized cellulose	Magnesium stearate
Titanium dioxide	HPMC 2910	
Macrogol 4000	Crosspovidon	Light anhydrous silicic acid

refraction. These observations indicate that features of a tablet's physical state resulting from the manufacturing process, such as the uneven distribution of granule sizes or the uneven penetration of compression force in a mortar, will change the density of tablet components.

In-Depth Terahertz Images

The depth (B-scan) terahertz images obtained from commercial tablets A–D are shown in Fig. 4. These tablets each have a coating thickness of approximately 100 μm. The left

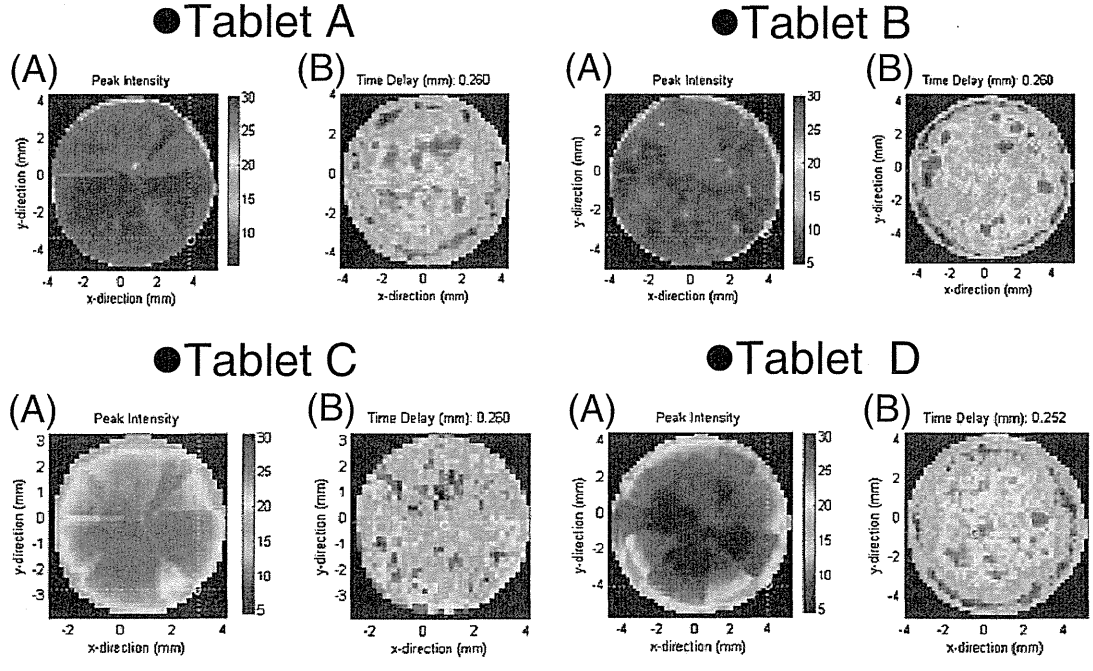

Fig. 3 Terahertz images of four different commercial tablets (**a** surface area and **b** at 0.26 mm depth from the surface)

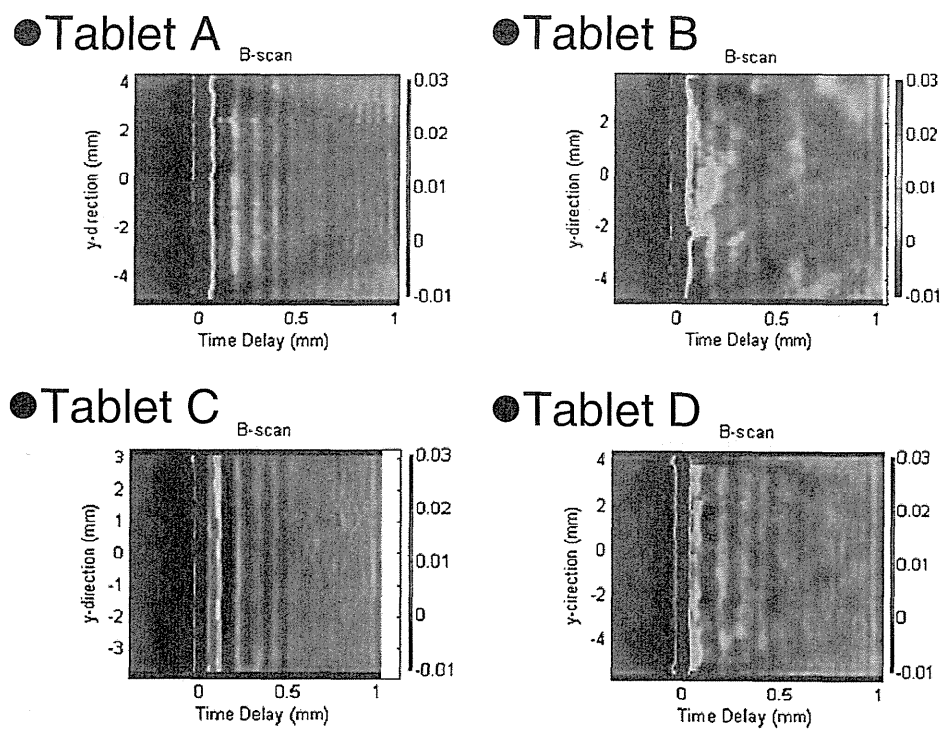

Fig. 4 Depth (*B-Scan*) terahertz images of four different commercial tablets (the area to the right of each brown line represents the inside of a tablet)

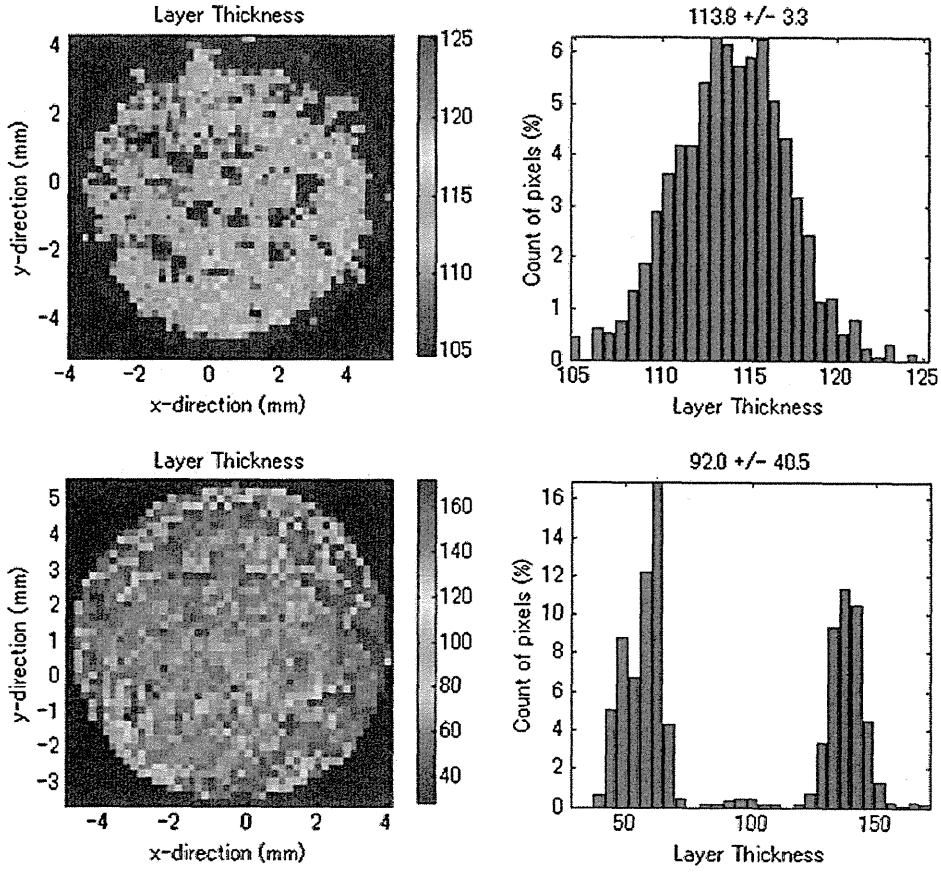

Fig. 5 Distribution of coating thickness (*left*) and histograms (*right*) (*upper images*, *Tablet A*; *lower images*, *Tablet D*)

and right sides of the brown line represent air and the inside of the tablet, respectively. The echoes showing several layers formed by compression are observed. Definite layers up to 1 mm depth and up to 0.5 mm depth appear in Tablets A and C, respectively. The indistinct echoes can be seen in Tablet D. On the other hand, indistinct but layer-like echoes are observed in Tablet B. Those observations suggest that unevenly penetrated compression force into the tablet. Further study is necessary to explain the details of these results. However, features of the pre-compression state, such as the particle size distribution of components in a mortar, would be affected by the penetration of compression force in the tablet compaction process. This physical property would be represented as echoes in depth terahertz images. Thus, a depth (B-scan) terahertz image would provide physical information about the effects of the manufacturing process on the tablet's state and also would sensitively detect changes in manufacturing quality.

Distribution of Coating Thickness

Figure 5 shows the distributions of coating thicknesses obtained from Tablets A and D. A histogram of the coating thickness of each tablet is shown at the right side of this figure. In the case of tablet A, the coating thickness was between 105 and 125 μm, a relatively narrow range of 20 μm. The coating thickness on the outer circuit of each tablet image shows a tendency toward relative thickness, and that on the center shows the opposite tendency. In the case of Tablet D, two peaks in the coating thickness range (40 to 70 and 120 to 150 μm) appear. Moreover, the thin and thick layers are irregularly distributed in the image. This observation definitely indicates that the coating property depends on the coating process. These results suggest that an inappropriate coating process was performed for tablet D.

Conclusions

A tablet containing relatively large amounts of API (from 75.1 to 82.3 %) would be detected qualitatively by comparison against the characteristic terahertz waveform of API. Terahertz imaging can reveal coating thicknesses and their distributions, the densities of components by compression, and hollows on a tablet surface based on the detection of the delayed reflection of terahertz pulses. Detection of the coating state and changes in the physical state, such as density distribution inside a tablet, would contribute not only to the identification of manufacturing quality but also to qualitative confirmation of commercial tablets including fake (counterfeit) and/or defective products. The TPS and imaging techniques will be useful as nondestructive analytical tools for the quality control of commercial tablets.

Acknowledgments This study was supported in part by a research grant from the Ministry of Health, Labour, and Welfare of Japan (H20-iyaku-ippan-004). The authors would like to thank Mr. Tsuyoshi Miura, Mr. Daisuke Sasakura, and Mr. Tomoyuki Matsubara (Bruker Optics K.K., Japan) for their kind assistance.

References

1. Korter TM, et al. Terahertz spectroscopy of solid serine and cysteine. Chem Phys Lett. 2006;418:65–70.
2. Day GM, et al. Understanding the influence of polymorphism on phonon spectra: lattice dynamics calculations and terahertz spectroscopy of carbamazepine. J Phys Chem B. 2006;110:447–56.
3. Allis DG, et al. Solid-state modeling of the terahertz spectrum of the high explosive HMX. J Phys Chem A. 2006;110:1951–9.
4. Saito S, et al. Terahertz vibrational modes of crystalline salicylic acid by numerical model using periodic density functional theory. Jpn J Appl Phys Part 1-Regul Pap Brief Commun Rev Pap. 2006;45:4170–5.
5. Saito S, et al. Terahertz phonon modes of an intermolecular network of hydrogen bonds in an anhydrous beta-D-glucopyranose crystal. Chem Phys Lett. 2006;423:439–44.
6. Allis DG, et al. Theoretical analysis of the terahertz spectrum of the high explosive PETN. Chem Phys Chem. 2006;7:2398–408.
7. Taday PF, et al. Using terahertz pulse spectroscopy to study the crystalline structure of a drug: a case study of the polymorphs of ranitidine hydrochloride. J Pharm Sci. 2003;92:831–8.
8. Walther M, et al. Noncovalent intermolecular forces in polycrystalline and amorphous saccharides in the far infrared. Chem Phys. 2003;288:261–8.
9. Strachan CJ, et al. Using terahertz pulsed spectroscopy to study crystallinity of pharmaceutical materials. Chem Phys Lett. 2004;390:20–4.
10. Zeitler JA, et al. Characterization of temperature induced phase transitions in the five polymorphic forms of sulfathiazole by terahertz pulsed spectroscopy and differential scanning calorimetry. J Pharm Sci. 2006;95:2486–98.
11. Zeitler JA, et al. Temperature dependent terahertz pulsed spectroscopy of carbamazepine. Thermochimica Acta. 2005;436:70–6.
12. Strachan CJ, et al. Using terahertz pulsed spectroscopy to quantify pharmaceutical polymorphism and crystallinity. J Pharm Sci. 2005;94:837–46.
13. Zeitler JA, et al. Relaxation and crystallization of amorphous carbamazepine studied by terahertz pulsed spectroscopy. J Pharm Sci. 2007;96:2703–9.
14. Kogermann K, et al. Investigating dehydration from compacts using terahertz pulsed, Raman, and near-infrared spectroscopy. Appl Spectrosc. 2007;61:1265–74.
15. Zeitler JA, et al. Characterization of drug hydrate systems and dehydration processes using terahertz pulsed spectroscopy. Int J of Pharmaceutics. 2007;334:78–84.
16. Liu H-B, et al. Characterization of anhydrous and hydrated pharmaceutical materials with THz time-domain spectroscopy. J Pharm Sci. 2007;96:927–34.

17. Ho L, et al. Analysis of sustained-release tablet film coats using terahertz pulsed imaging. J Control Release. 2007;119:253–61.
18. Ho L, et al. Applications of terahertz pulsed imaging to sustained-release tablet film coating quality assessment and dissolution performance. J Control Release. 2008;127:79–87.
19. Ho L, et al. Terahertz pulsed imaging as an analytical tool for sustained-release tablet film coating. Eur J Pharm Biopharm. 2009;71:117–23.
20. Fitzgerald AJ, et al. Nondestructive analysis of tablet coating thicknesses using terahertz pulsed imaging. J Pharm Sci. 2005;94:177–83.
21. Zeitler JA, et al. Analysis of coating structures and interfaces in solid oral dosage forms by three dimensional terahertz pulsed imaging. J Pharm Sci. 2007;96:330–40.
22. Sakamoto T, et al. Detection of tulobuterol crystal in transdermal patches using terahertz pulsed spectroscopy and imaging. Pharmazie. 2009;64:361–5.

Analytical Biochemistry 420 (2012) 61–67

Contents lists available at SciVerse ScienceDirect

Analytical Biochemistry

journal homepage: www.elsevier.com/locate/yabio

Analysis of oligomeric stability of insulin analogs using hydrogen/deuterium exchange mass spectrometry

Shiori Nakazawa [a,b], Noritaka Hashii [a,*], Akira Harazono [a], Nana Kawasaki [a,b]

[a] Division of Biological Chemistry and Biologicals, National Institute of Health Sciences, 1-18-1 Kami-yoga, Setagaya-ku, Tokyo 158-8501, Japan
[b] Graduate School of Life Science, Hokkaido University, Kita 12-Nishi 6, Kita-ku, Sapporo 060-0812, Japan

ARTICLE INFO

Article history:
Received 8 July 2011
Received in revised form 9 August 2011
Accepted 1 September 2011
Available online 7 September 2011

Keywords:
Insulin
HDX/MS
Oligomeric stability

ABSTRACT

Insulin analog products for subcutaneous injection are prepared as solutions in which insulin analog molecules exist in several oligomeric states. Oligomeric stability can affect their onset and duration of action and has been exploited in designing them. To investigate the oligomeric stability of insulin analog products having different pharmacokinetics, we performed hydrogen/deuterium exchange mass spectrometry (HDX/MS), which is a rapid method to analyze dynamic aspects of protein structures. Two rapid-acting analogs (lispro and glulisine) incorporated deuteriums more and faster than recombinant human insulin, whereas a long-acting analog (glargine) and two intermediate-acting preparations (protamine-containing formulations) incorporated them less and more slowly. Kinetic analysis revealed that the number of slowly exchanged hydrogens (D_s) ($k < 0.01$ min^{-1}) accounted for the difference in HDX reactivity among analogs. Furthermore, we found correlations between HDX kinetics and pharmacokinetics reported previously. Their maximum serum concentration (C_{max}) was linearly correlated with D_s ($r = 0.88$) and the number of maximum exchangeable hydrogens (D_∞) ($r = 0.89$). The maximum drug concentration time (t_{max}) was also correlated with reciprocals of D_s and D_∞ ($r = 0.86$ and $r = 0.96$, respectively). Here we demonstrate the ability of HDX/MS to evaluate oligomeric stability of insulin analog products.

Insulin is a peptide hormone consisting of two peptides: an A chain with 21 amino acids and a B chain with 30 amino acids. Insulin is the only hormone in vertebrates to induce cellular uptake of glucose and lower blood glucose levels, and it is an essential drug for treating diabetes mellitus.

As a drug product, insulin molecules primarily form hexamers, which diffuse and dilute in the subcutaneous tissue after injection [1] and dissociate into monomers via dimers or tetramers [1,2]. Monomeric insulin is absorbed into microvessels to exert its pharmacological action [3]. Therefore, oligomeric stability is a crucial property of insulin, determining its onset and duration of action (Fig. 1).

To mimic the intrinsic insulin secretion and enable better control of blood glucose levels, several recombinant human insulin analogs with different onset and duration of action have been developed and marketed. Compared with the basic preparation of recombinant human insulin, insulin analog products are generally categorized on the basis of differences in the onset and duration of their action—rapid-acting, long-acting, and intermediate-acting groups. Fig. 2 and Table 1 present the primary structures and several characteristics of insulin analogs investigated in this study [4–6]. Insulin lispro (lispro) is a rapid-acting insulin analog in which the positions of proline at B28 and lysine at B29 are reversed. Insulin glulisine (glulisine) is another major rapid-acting analog in which asparagine and lysine at positions B3 and B29 are replaced by lysine and glutamic acid, respectively. The amino acid substitutions in lispro and glulisine lead to a decrease in oligomeric stability; therefore, they act rapidly after subcutaneous injection. Insulin glargine (glargine) is a long-acting analog in which asparagine at position 21 on the A chain is substituted by glycine and two arginine residues are added to the C terminus of the B chain. Glargine has a higher isoelectric point (6.7) [7,8] than human insulin and its analogs, which range from 5.0 to 5.5 [9–12]. Glargine formulated at pH 3.5 to 4.5 precipitates in neutral conditions after subcutaneous injection [13,14]. Its precipitant gradually dissociates and is absorbed slowly into the bloodstream, and thereby glargine has a slower onset and longer duration of action than human insulin. Insulin detemir (detemir) is another type of long-acting analog that was designed with a concept different from modification of oligomeric stability. Detemir, in which a myristic acid is covalently bound to lysine at B29, binds to albumin in subcutaneous tissues and plasma. This modification leads to delay in absorption and prolongation of the serum half-life. The intermediate-acting group is another type of insulin with longer action in which the hexameric insulin (analog) is stabilized by forming a

* Corresponding author. Fax: +81 3 3700 9084.
E-mail address: hashii@nihs.go.jp (N. Hashii).

0003-2697/$ - see front matter © 2011 Elsevier Inc. All rights reserved.
doi:10.1016/j.ab.2011.09.002

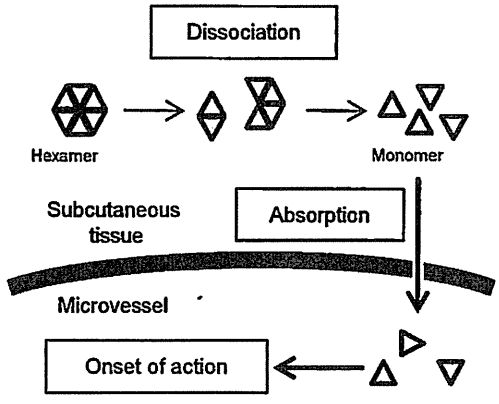

Fig.1. Absorption of subcutaneously injected insulin. Insulin molecules in drug products exist mainly as hexamers. After subcutaneous injection, diluted hexamers dissociate to monomers to be absorbed by microvessels.

Fig.2. Primary structures of insulin analogs we examined. Dashed lines represent disulfide bonds. Mutated residues are underscored.

Table 1
Human insulin and its analog products examined in this study.

Group	Analog	Onset of action	Duration of action	Molecular weight	pI	pH of drug product
	Human Insulin	30–60 min	4–12 h	5807.57	5.4	7.0–7.8
Rapid	Lispro	5–15 min	4–6 h	5807.57	5.65	7.0–7.8
	Glulisine	5–15 min	1–2.5 h	5822.58	5.1	7.0–7.8
Long	Glargine	2–4 h	20–24 h	6062.89	6.7	3.5–4.5
	Detemir	2 h[a]	6–24 h[a]	5916.82		7.2–7.6
Intermediate	NPH	2–4 h	10–16 h	5807.57		7.0–7.5
	NPL	1–2 h	10–16 h	5807.57		7.0–7.8

[a] Dose dependent.

complex with protamine to suppress dissociation in subcutaneous tissue after injection. Human isophane insulin (neutral protamine

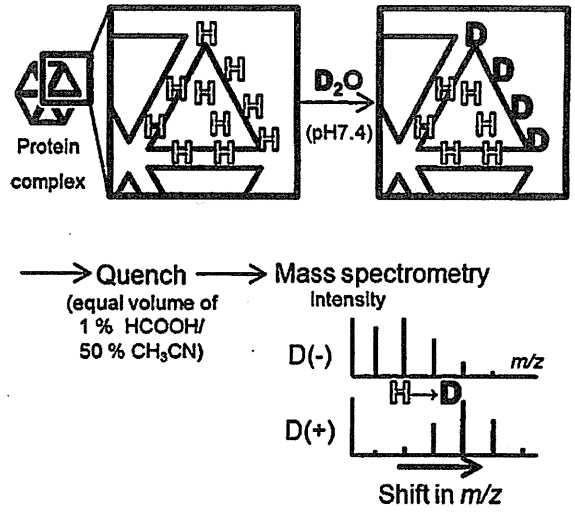

Fig.3. Schematic model of HDX/MS. The protein sample is exposed to deuterated solvent and subjected to MS. Hydrogen atoms, without participating in hydrogen bonds or any other noncovalent bonds, are more easily exchanged with deuteriums. Exchanged deuteriums are detected as the shift in *m/z* value distributions.

Hagedorn, NPH)[1] and a lispro preparation containing protamine (neutral protamine lispro, NPL) belong to the intermediate-acting group.

Evaluation of oligomeric states of formulated insulin analogs is important to support their appropriate use. Previously, the oligomeric states of insulin analogs were determined by sedimentation velocity or static light scattering or were estimated by comparing their circular dichroism spectra under different conditions [15]. However, the oligomeric stability of these formulated insulin analogs have not been investigated because of the absence of convenient methods. Therefore, there is an increasing need for an easy, rapid, and accurate method to evaluate stability of the association state of insulin.

Hydrogen/deuterium exchange mass spectrometry (HDX/MS) is a known method to analyze structural fluctuations of proteins [16–18]. HDX/MS is based on the exchange reaction between hydrogens in proteins and deuteriums in the D_2O solvent. A protein sample is incubated in a D_2O solvent to incorporate deuteriums, and then the sample solution is mixed with an acidic reagent to suppress the HDX reaction. The number of incorporated deuteriums is calculated from the difference in the average mass obtained by liquid chromatography mass spectrometry (LC/MS) before and after the HDX reaction (Fig. 3). Deuteriums that were exchanged with amide hydrogens in the protein backbone are primarily detected by HDX/MS because hydrogens in protein side chain groups (e.g., –OH, $–NH_2$, –SH, –COOH, $–CONH_2$) have lower pK_a values, have higher exchange rates even after the addition of H^+, and undergo a back-exchange reaction to lose deuteriums [19]. The exchange rate of each amide hydrogen depends on its interaction with the solvent [20–22]. A moiety with more structural fluctuations, which is not involved in an α-helix or a β-sheet, not packed in the hydrophobic core, and not trapped in other interactions, has more solvent accessibility. Thus, a moiety or molecule that interacts with the solvent further (e.g., a monomer vs. an oligomer) will gain more exchanged deuteriums [23].

[1] *Abbreviations used:* NPH, neutral protamine Hagedorn; NPL, neutral protamine lispro; HDX/MS, hydrogen/deuterium exchange mass spectrometry; LC/MS, liquid chromatography mass spectrometry; HPLC, high-performance liquid chromatography; PCA, principal component analysis; DSL, dynamic light scattering.

HDX/MS can potentially be applied to estimate the stability of insulin oligomers.

In this study, we compared the HDX reactivity of insulin analog formulations with different oligomeric stability and different drug dispositions. We found correlations between their HDX kinetic parameters and their pharmacokinetic parameters. Here we demonstrate the usefulness of HDX/MS to evaluate oligomeric stability of insulin analog products and propose its potential use for predicting their onset and duration of action.

Materials and methods

Materials

Human insulin (Humulin R), insulin lispro (Humalog), NPH insulin (Humulin N), and NPL (Humalog N) were purchased from Eli Lilly (Indianapolis, IN, USA). Insulin glargine (Lantus) and insulin glulisine (Apidra) were purchased from Sanofi–Aventis (Paris, France). Insulin detemir (Levemir Penfill) was purchased from Novo Nordisk (Bagsværd, Denmark). All compounds were provided at a concentration of 100 U/ml, approximately 3.5 mg/ml (0.61 mM). Ammonium acetate and formic acid were purchased from Wako Pure Chemical Industries (Osaka, Japan). Acetonitrile and D_2O were purchased from Sigma–Aldrich (St. Louis, MO, USA).

HDX/MS

Protein solutions were diluted 10-fold with 10 mM ammonium acetate in 90% D_2O (pH 7.4) and kept on ice during the HDX reaction because conducting the reaction at room temperature resulted in a very high exchange rate that made it difficult to successfully observe a time-dependent change. Final concentrations of insulin analogs were approximately 60 mM (0.35 mg/ml). At each time point, 50 µl of the reaction solution was mixed with an equal volume of ice-chilled formic acid/acetonitrile/water (1:49:50) to repress the exchange reaction; this step is called "quenching." Deuterated proteins were introduced into the mass spectrometer with the Paradigm MS4 HPLC (high-performance liquid chromatography) system (Michrom BioResoruces, Auburn, CA, USA) through an L-column Micro trap column with C18 solid phase (Chemicals Evaluation and Research Institute, Tokyo, Japan) at a flow rate of 50 µl/min over 10 min with 0.1% formic acid in 50% acetonitrile. Mass spectra were recorded using a Fourier transform ion cyclotron resonance mass spectrometer (LTQ-FT, Thermo Fisher Scientific, Waltham, MA, USA) equipped with a nanoelectrospray ion source (AMR, Tokyo, Japan). The conditions for MS analysis were as follows: an electrospray voltage of 2.5 kV in positive ion mode, a capillary temperature of 200 °C, and an m/z range of 1000 to 4000. The number of incorporated deuteriums was determined by subtraction of the weight-average molecular weights.

Table 2
Hydrodynamic diameters of insulin analogs in 10 mM ammonium acetate (pH 7.4).

	Concentration (µM)			
	15	30	60	120
Insulin	4.7 ± 0.1	5.1 ± 0.3	4.7 ± 0.1	4.6 ± 0.1
Lispro	3.2 ± 0.4	3.6 ± 0.6	4.4 ± 0.2	4.6 ± 0.1
Glulisine	3.3 ± 0.6	3.7 ± 0.2	4.5 ± 0.1	4.5 ± 0.3
Glargine	609.1 ± 42.8	284.2 ± 8.2	274.0 ± 28.0	4.9 ± 0.1
Detemir	13.2 ± 0.1	11.0 ± 2.9	6.2 ± 0.0	5.4 ± 0.1
Insulin/H^+			2.6 ± 1.0	

Note. Values are mean diameters (nm) ± standard deviations (n = 3).

Table 3
Relative volume in neutral buffer compared with that of human insulin in acidic solution.

	Concentration (µM)			
	15	30	60	120
Insulin	5.9	7.6	6.2	5.8
Lispro	1.9	2.8	5.1	5.5
Glulisine	2.1	2.9	5.4	5.3
Glargine	1.3×10^7	1.3×10^6	1.2×10^6	6.8
Detemir	131.6	77.2	14.0	9.2

Note. Relative volume (to insulin/H^+) was calculated as (mean diameter of each analog at each concentration)^3/(mean diameter of insulin/H^+)^3.

Table 4
HDX kinetics of insulin analogs.

	Number of exchangeable hydrogens				
	Maximum (D_∞)	(D_0)	Slow (D_s)	Medium (D_i)	Fast (D_f)
Insulin	20.3	(11.9)	3.9	1.5	3.0
Lispro	24.5	(12.2)	7.3	2.6	2.5
Glulisine	24.7	(12.1)	7.2	2.6	2.8
Glargine	18.0	(10.1)	2.0	1.8	4.2
Detemir	19.9	(12.7)	3.3	1.6	2.5
NPH	16.4	(9.9)	1.0	1.8	3.6
NPL	16.9	(11.8)	1.3	2.0	1.8

Note. Shown are numbers of maximum exchangeable hydrogens and slow-exchanging ($k \leq 0.1\ min^{-1}$), intermediate-exchanging ($0.1 < k \leq 1$), or fast-exchanging ($k > 1.0$) hydrogens that were calculated on the basis of Eq. (1). D_t values of when $t = 0$ are in parentheses.

Calculation of kinetic parameters

The modeling and calculation of deuterium incorporation were done using Mathcad 14.0 software (PTC, Needham, MA, USA). Details of fitting with Eq. (1) are described in Results.

Size distribution measurements

Hydrodynamic diameter distributions were determined with the dynamic light scattering method by Zetasizer Nano (Malvern Instruments, Worcestershire, UK). Insulin analog products were diluted with 10 mM ammonium acetate (pH 7.4) to 15, 30, 60, and 120 µM. Acidic solution of insulin for the control was prepared with Humulin R and a 9-fold volume of 0.1% formic acid, which had a final pH of 2.7 at 25.7 °C. Overnight equilibration was performed at 4 °C prior to measurements. The relative volume given in Table 3 was calculated as the cube of the ratio of the mean diameter to that of insulin/H^+.

Multivariate analysis

Principal component analysis (PCA) was performed using SIMCA-P$^+$ software (Umetrics, Umeå, Sweden) with the PCA method. As the variables, the numbers of maximum exchangeable hydrogens (D_∞), and slow- and intermediate-exchanging hydrogens (D_s and D_i, respectively) (Table 4) were input. Before input, the variables were divided by the number of amide hydrogens in the main chains of each analog.

Results

Hydrodynamic diameter distributions of insulin analog products

To confirm the oligomeric states of insulin analogs used in this study, the particle size of four analogs (lispro, glulisine, glargine, and detemir) were measured by dynamic light scattering (DLS) after dilution of these analogs with an H_2O solvent of the same

composition as HDX solvent (Tables 2 and 3). As a control, an acidic solution of 60 μM human insulin (insulin/H^+), in which insulin exists mainly as a mixture of monomers and dimers, was prepared [24]. At a high concentration (120 μM), the mean diameters of the four analogs obtained by DLS were similar to that of human insulin. In addition, their volumes calculated from the mean diameters were 6-fold larger than that of insulin/H^+ (Table 3), suggesting that they could exist as hexamers at a high concentration.

At lower concentrations (15 and 30 μM), the mean diameters of the two rapid-acting analogs, lispro and glulisine, were smaller than the diameters at higher concentrations, although the diameter of human insulin remained roughly constant at all concentrations. These data indicate that the rapid-acting analogs dissociate more rapidly than human insulin. Glargine, with an isoelectric point of 6.7, showed an increase in diameter with a decrease in concentration by dilution with a neutral solvent, indicating the aggregation of glargine molecules. At lower concentrations (15 μM), detemir formed large particles approximately 130 times larger than insulin/H^+, possibly suggesting the association of detemir molecules at lower concentrations. These results are consistent with the prevailing oligomeric stability of insulin analogs except for detemir.

HDX/MS of human insulin and insulin analogs

First, to determine deuterium incorporation by human insulin as the standard, human insulin was subjected to the HDX reaction and LC/MS as described in Materials and Methods. To conduct exchange reaction under physiological pH conditions, we selected

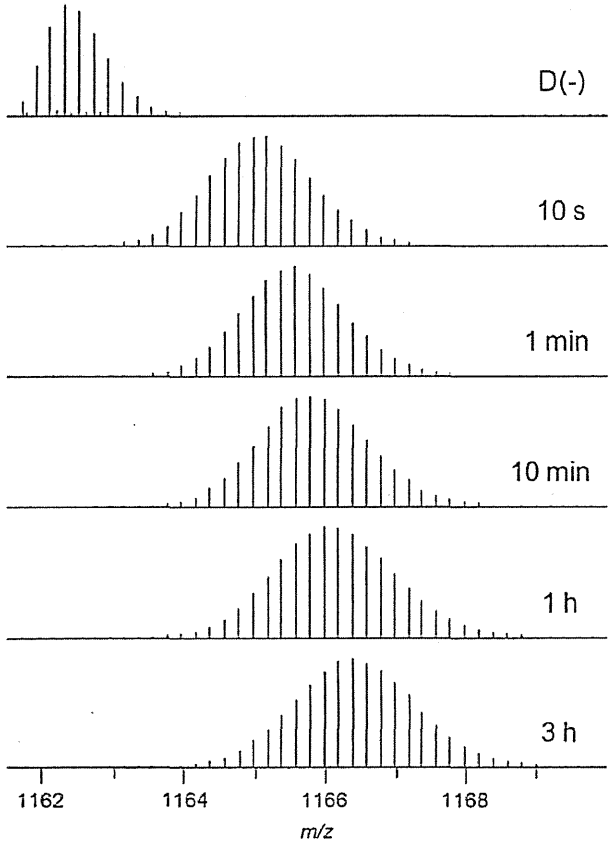

Fig.4. Representative mass spectra of human insulin observed during the HDX procedure. The original spectrum of human insulin without deuterium label [D(−)] and spectra obtained at several time points of HDX reaction are shown.

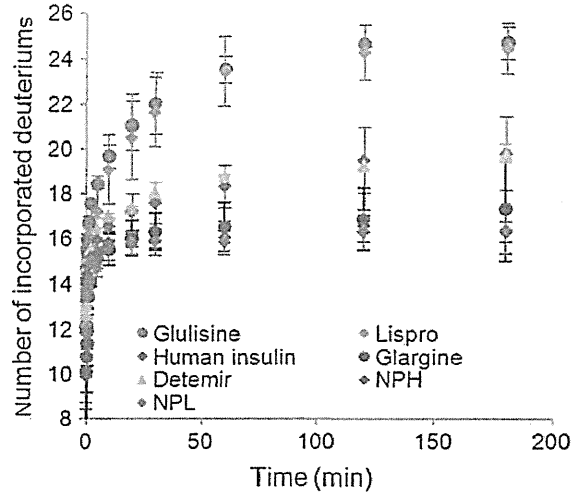

Fig.5. Time-series plot of deuterium uptake by insulin analog products.

ammonium acetate buffer, one of the better buffers to mimic in vivo pH condition, considering applicability to the mass spectrometer. The time-dependent shift of the mass spectra and the number of incorporated deuteriums by human insulin are shown in Figs. 4 and 5 (red rhombus). The uptake was fast during the first 5 min, and approximately 80% of the incorporation was complete within the first minute. After 3 h of the HDX reaction, the number of incorporated deuteriums was 19.82 ± 1.64 (mean ± standard deviation, $n = 4$).

Next, to determine whether the HDX reactivity of rapid-, long-, or intermediate-acting insulin analogs differed from that of human insulin, six analog products were examined (Fig. 5). Lispro and glulisine exhibited higher exchange reactivity than human insulin (24.48 ± 1.10 and 24.74 ± 0.70, respectively, after a 3 h reaction, $n = 3$), but glargine showed lower exchange reactivity than human insulin (17.57 ± 0.42 after 3 h, $n = 3$), indicating its enhanced oligomeric stability. Similarly, two formulations of the intermediate-acting group, NPH and NPL, also had lower reactivity (16.32 ± 0.43 and 16.39 ± 1.03, respectively, after 3 h, $n = 3$). Unlike the other analogs, detemir had a similar number of incorporated deuteriums as human insulin (19.84 ± 0.40 after 3 h, $n = 3$).

Kinetics of HDX reactivity of insulin analogs

To obtain further information on the oligomeric stability of insulin analogs, we investigated the kinetics of HDX reactions of human insulin and the insulin analogs. In general, HDX reactions of proteins can be modeled as a pseudo-first-order reaction [21], and exchangeable amide hydrogens are classified into three kinetic groups: fast-, intermediate-, and slow-exchanging hydrogens [25]. On these bases, we calculated the kinetics using Eq. (1), a tetranomial function of reaction time (t) defined by reaction rate constants of each hydrogen group (k_f, k_i, and k_s), denoting the maximum number of exchangeable hydrogen atoms by D_∞, and the number of hydrogens of each kinetic group by D_f, D_i, and D_s. The latter three terms represent the hydrogens that have not been exchanged after a t-min reaction. We employed the tetranomial model because it gave higher values of Pearson correlation coefficients than modeling with three or five terms:

$$D_t = D_\infty - D_f \exp(-k_f t) - D_i \exp(-k_i t) - D_s \exp(-k_s t). \quad (1)$$

The sets of coefficients (D_f, D_i, D_s, and D_∞) and reaction rate constants (k_f, k_i, and k_s) that gave the highest Pearson correlation coefficients were sought by fitting the mean number of incorporated

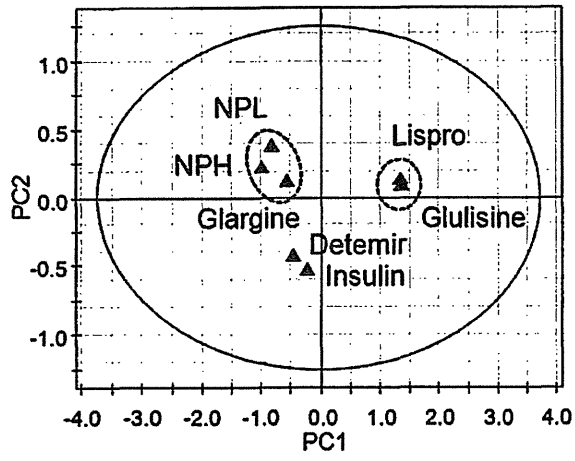

Fig.6. The score plot for the PCA of the HDX kinetic parameters. Primary (PC1) and secondary (PC2) principal components are indicated.

Table 5
Reported values of C_{max} and t_{max}.

Analog	C_{max} (μU/ml)	t_{max} (min)	Reference
Insulin	43.3	109	[26]
	35.8	97.5	[27]
	40.0	104	[28]
	46.0	92	[28]
	46.0	82	[29]
	51.1	101	[11]
Lispro	147.2	71	[30]
	81.0	71	[28]
	91.4	53	[11]
Glulisine	73.0	57	[28]
	92.0	83	[28]
	82.0	55	[29]
Glargine	18.9	180	[31]
NPH	13.5		[32]
	20.0		[32]
	22.8	360	[31]
NPL	21.3	200	[30]

Note. Shown are reported values of C_{max} and t_{max} in studies about insulin analog products [11,26–32]. Glargine's t_{max} was deduced from the time-concentration plot in Ref. [31].

deuteriums at every observed time point to Eq. (1). The resulting values for D_f, D_i, D_s, and D_∞ are shown in Table 4. The fast-acting group had the highest D_∞, followed by the human insulin, long-acting, and intermediate-acting groups. Interestingly, the number of hydrogens that were already exchanged at the beginning of the HDX reaction (D_t when $t = 0$) was not different among the respective groups, suggesting that differences in D_∞ originated from hydrogens that had lower exchange reaction rates and, therefore, were not exchanged during the first few seconds. Furthermore, D_s of the rapid-acting analogs were increased compared with those of the other groups. From these results, the number of D_s could be related to the difference in the overall HDX reactivity among insulin analogs.

PCA using HDX kinetic parameters of insulin analogs

We examined whether rapid-, long-, and intermediate-acting groups were distinguished by PCA using the HDX kinetic parameters, D_∞, D_f, D_i, and D_s. The score plots for PC1 and PC2 are shown in Fig. 6. Lispro and glulisine were plotted at neighboring positions, distant from human insulin and other analogs. In addition, three preparations with a lower tendency for dissociation (i.e., glargine, NPH, and NPL) were plotted closely together. However, detemir was plotted near human insulin, not near analogs of the long-acting group. This result demonstrates that the insulin analogs with different pharmaceutical properties are distinguished by their HDX reactivity.

Pharmacokinetic parameters and HDX kinetics of insulin analogs

We analyzed the association between the HDX kinetic parameters and the actual pharmacokinetic parameters in humans. We compared previously reported values [11,26–32] of the maximum plasma concentrations (C_{max}) and the maximum drug concentration time (t_{max}) after subcutaneous injection with our kinetic parameters, D_∞, D_s, D_i, and D_f (Table 5). Detemir, employing the affinity to albumin instead of the oligomeric stability for its longer action, was excluded. C_{max} had linear correlations with D_∞ and D_s ($r = 0.88$ and $r = 0.89$, respectively) (Fig. 7A). In addition, t_{max} correlated with reciprocals of D_∞ and D_s ($r = 0.86$ and $r = 0.96$, respectively) (Fig. 7B).

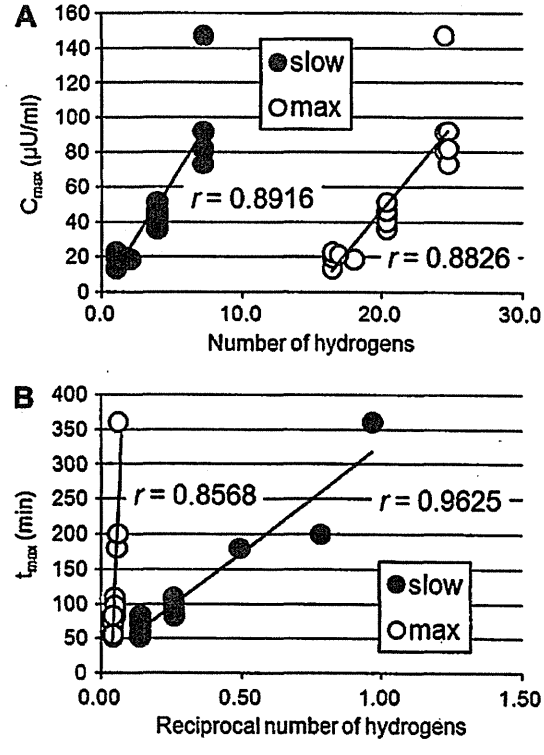

Fig.7. Relations between HDX kinetic parameters and C_{max} (A) or t_{max} (B) values.

Discussion

Since insulin lispro was first sold in 1995 as an analog of recombinant human insulin, many insulin analog products have been marketed. Oligomeric stability of formulated analogs is important for controlling their onset and duration of action. In this study, we analyzed the oligomeric stability of formulated insulin analogs by HDX/MS, which is an analytical method to determine structural fluctuations of proteins, and we investigated relationships between the parameters of HDX kinetics and pharmacokinetics of the analogs.

We first measured the diameters of the formulated insulin analogs under the same conditions as the HDX reaction. The diameters of two rapid-acting analogs (lispro and glulisine), which have low oligomeric stability, were smaller than that of human insulin at low concentrations, although glargine, a long-acting analog, formed large aggregates with an increase in pH by neutralization (Fig. 4). These results are consistent with previous studies and provide evidence that rapid-acting analogs dissociate more easily than human insulin and glargine forms aggregates at physiological pH. Detemir, another long-acting analog, exhibited unique behavior. It did not form huge aggregates like glargine, but it had larger diameters with dilution; its mean diameters were 2- or 3-fold larger than those of human insulin. This would have resulted from the suggested complex of detemir hexamers mediated by their acyl chains [33,34].

Next, we determined the HDX reactivity of human insulin and insulin analogs of rapid-, long-, and intermediate-acting groups (Fig. 5). Lispro and glulisine incorporated more deuteriums than human insulin. On the other hand, glargine and two products of the intermediate-acting group (NPH and NPL) incorporated fewer deuteriums than human insulin. These results demonstrate that HDX reactivity of insulin analogs at neutral pH were associated with their oligomeric stability. Interestingly, detemir, in spite of its prolonged action, had exchange reactivity similar to that of human insulin. Considering the mechanism in which detemir hexamers associate, there could be little effect on the solvent accessibility of peptide moieties of detemir molecules even when their hexamers form a larger complex.

The PCA using kinetic parameters of the HDX reactions resulted in a distinction among the three groups (Fig. 6). Two analogs of the rapid-acting group, one long-acting preparation, and two intermediate-acting preparations were plotted at close positions. However, detemir was plotted far from the other analogs of long- and intermediate-acting groups and was closer to human insulin. This result was in agreement with the time-dependent incorporation of deuteriums (Fig. 4). We suggest that only four kinetic parameters (D_∞, D_f, D_i, and D_s) obtained by HDX/MS allow for discrimination of insulin analogs of different groups. In addition, PCA using the kinetic parameters could also be applicable to evaluate similarities in similar biological medicinal products of insulin analogs under development.

We analyzed the association between the HDX kinetic parameters and the actual pharmacokinetic parameters in humans. We compared previously reported values of C_{max} and t_{max} (Table 5) with our kinetic parameters (Table 4). This resulted in the correlations with D_∞ and D_s shown in Fig. 7. These results suggest that D_∞ and D_s could be useful as characteristic markers for prediction of C_{max} and t_{max}. In a previous study on HDX with human insulin and lispro reported by Chitta and coworkers [25], D_∞ values were nearly equal to the total number ($D_f + D_i + D_s$) of amide deuteriums in the peptide backbone. However, in our study, the total number of D_f, D_i, and D_s was from 30% to 51% of D_∞, indicating that there could be some deuteriums left in side chains. Differences from the previous study could be caused by the difference in the temperature at which the HDX reaction was performed. In other words, continuous cooling through the entire procedure of HDX to moderate the exchange reaction in our study could account for the differences. Chitta and coworkers also reported a difference in D_i between human insulin and lispro [25], whereas in our study the only difference was observed in the D_s numbers. On ice, incubation could have switched some of the fast hydrogens to intermediate hydrogens and switched some of the intermediate hydrogens to slow hydrogens.

The concentration of insulin is a significant factor that affects the association and dissociation of insulin oligomer [24] and, thus, also affects the HDX reactivity [25]. When comparing the oligomeric stability of insulin preparations by HDX/MS, one should be careful about sample concentration because the difference in HDX reactivity could attenuate if insulin concentration were too high to dissociate (or too low to form even dimer).

Finally, we demonstrated the utility and capability of the HDX/MS method for evaluating the oligomeric stability of insulin analog products. We also revealed relationships between some HDX kinetic parameters and pharmacokinetic parameters. We believe that our current method could be helpful in predicting the pharmacokinetics of insulin analogs.

Acknowledgment

This study was supported in part by a Grant-in-Aid from the Ministry of Health, Labour, and Welfare (Japan).

References

[1] J. Brange, D.R. Owens, S. Kang, A. Volund, Monomeric insulins and their experimental and clinical applications, Diabetes Care 13 (1990) 923–954.
[2] M.R. DeFelippis, R.E. Chance, B.H. Frank, Insulin self-association and the relationship to pharmacokinetics and pharmacodynamics, Crit. Rev. Ther. Drug Carrier Syst. 18 (2001) 201–264.
[3] J. Brange, A. Volund, Insulin analogs with improved pharmacokinetic profiles, Adv. Drug Deliv. Rev. 35 (1999) 307–335.
[4] J.A. Mayfield, R.D. White, Insulin therapy for type 2 diabetes: rescue, augmentation, and replacement of beta-cell function, Am. Fam. Physician 70 (2004) 489–500.
[5] S.N. Charugulla, T.S. Kamat, K. Peetambaran, V.M. Thorat, Insulin analogues: an update, Res. J. Krishna Inst. Karad 2 (2009) 6–12.
[6] NIH Daily Med, HUMULIN (insulin human) injection, solution (Eli Lilly and Company). 2011. Available from: <http://dailymed.nlm.nih.gov/dailymed/druginfo.cfm?id=43212>.
[7] C. Binder, A theoretical model for the absorption of soluble insulin, in: P. Brunetti (Ed.), Artificial Systems for Insulin Delivery, Raven, New York, 1983, pp. 53–57.
[8] C.J. Dunn, G.L. Plosker, G.M. Keating, K. McKeage, L.J. Scott, Insulin glargine: an updated review of its use in the management of diabetes mellitus, Drugs 63 (2003) 1743–1778.
[9] O. Wintersteiner, H.A. Abramson, The isoelectric point of insulin, J. Biol. Chem. 99 (1993) 741–753.
[10] T. Blundell, G. Dodson, D. Hodgkin, D. Mercola, Insulin: the structure in the crystal and its reflection in chemistry and biology, Adv. Protein Chem. 26 (1972) 279–402.
[11] Eli Lilly Canada, Humalog product monograph. 2011. Available from: <http://www.lilly.ca/servlets/sfs;jsessionid=2606BA9CBC69DD8DCF6B024A9D13FE897t=/documentManager/sfdoc.file.supply&e=UTF-8&i=1233164768976&l=0&s=2S4REX2uNLETAStSC&fileID=1299285990234>.
[12] European Medicines Agency Committee for Medicinal Products for Human Use, Apidra: European Public Assessment Report—Scientific Discussion. 2011. Available from: <http://www.ema.europa.eu/ema/index.jsp?curl=pages/medicines/human/medicines/000557/human_med_000648.jsp&murl=menus/medicines/medicines.jsp&mid=WC0b01ac058001d125#>.
[13] G.B. Bolli, D.R. Owens, Insulin glargine, Lancet 356 (2000) 443–445.
[14] U. Dashora, V. Dashora, Insulin glargine, Int. J. Diabetes Dev. Countries 20 (2000) 140–144.
[15] D.L. Bakaysa, J. Radziuk, H.A. Havel, M.L. Brader, S. Li, S.W. Dodd, J.M. Beals, A.H. Pekar, D.N. Brems, Physicochemical basis for the rapid time-action of $Lys^{B28}Pro^{B29}$-insulin: dissociation of a protein-ligand complex, Protein Sci. 5 (1996) 2521–2531.
[16] A. Hvidt, K. Linderstrøm-Lang, Exchange of hydrogen atoms in insulin with deuterium atoms in aqueous solutions, Biochim. Biophys. Acta 14 (1954) 574–575.
[17] S.W. Englander, L. Mayne, Y. Bai, T.R. Sosnick, Hydrogen exchange: the modern legacy of Linderstrøm-Lang, Protein Sci. 6 (1997) 1101–1109.
[18] Y. Hamuro, S.J. Coales, M.R. Southern, J.F. Nemeth-Cawley, D.D. Stranz, P.R. Griffin, Rapid analysis of protein structure and dynamics by hydrogen/deuterium exchange mass spectrometry, J. Biomol. Tech. 14 (2003) 171–182.
[19] X. Yan, J. Watson, P.S. Ho, M.L. Deinzer, Mass spectrometric approaches using electrospray ionization charge states and hydrogen–deuterium exchange for determining protein structures and their conformational changes, Mol. Cell. Proteomics 3 (2003) 10–23.
[20] S.W. Englander, D.B. Calhoun, J.J. Englander, N.R. Kallenbach, R.K. Liem, E.L. Malin, C. Mandal, J.R. Rogero, Individual breathing reactions measured in hemoglobin by hydrogen exchange methods, Biophys. J. 32 (1980) 577–589.
[21] Z.Q. Zhang, D.L. Smith, Determination of amide hydrogen exchange by mass spectrometry: a new tool for protein structure elucidation, Protein Sci. 2 (1993) 522–531.
[22] J.R. Engen, D.L. Smith, Investigating protein structure and dynamics by hydrogen exchange MS, Anal. Chem. 73 (2001) 256A–265A.

[23] H. Maity, W.K. Lim, J.N. Rumbley, S.W. Englander, Protein hydrogen exchange mechanism: local fluctuations, Protein Sci. 12 (2003) 153–160.
[24] E.J. Nettleton, P. Tito, M. Sunde, M. Bouchard, C.M. Dobson, C.V. Robinson, Characterization of the oligomeric states of insulin in self-assembly and amyloid fibril formation by mass spectrometry, Biophys. J. 79 (2000) 1053–1065.
[25] R.K. Chitta, D.L. Rempel, M.A. Grayson, E.E. Remsen, M.L. Gross, Application of SIMSTEX to oligomerization of insulin analogs and mutants, J. Am. Soc. Mass Spectrom. 17 (2006) 1526–1534.
[26] S.R. Mudaliar, F.A. Lindberg, M. Joyce, P. Beerdsen, P. Strange, A. Lin, R.R. Henry, Insulin aspart (B28 asp-insulin): a fast-acting analog of human insulin—absorption kinetics and action profile compared with regular human insulin in healthy nondiabetic subjects, Diabetes Care 22 (1999) 1501–1506.
[27] A. Lindholm, J. McEwen, A.P. Riis, Improved postprandial glycemic control with insulin aspart: a randomized double-blind cross-over trial in type 1 diabetes, Diabetes Care 22 (1999) 801–805.
[28] R.H. Becker, A.D. Frick, Clinical pharmacokinetics and pharmacodynamics of insulin glulisine, Clin. Pharmacokinet. 47 (2008) 7–20.
[29] European Medicines Agency Committee for Medicinal Products for Human Use, Apidra: European Public Assessment Report—Product Information, 2011. Available from: <http://www.ema.europa.eu/docs/en_GB/document_library/EPAR_-_Product_Information/human/000557/WC500025250.pdf>.
[30] T. Heise, C. Weyer, A. Serwas, S. Heinrichs, J. Osinga, P. Roach, J. Woodworth, U. Gudat, L. Heinemann, Time–action profiles of novel premixed preparations of insulin lispro and NPL insulin, Diabetes Care 21 (1998) 800–803.
[31] M. Lepore, S. Pampanelli, C. Fanelli, F. Porcellati, L. Bartocci, A.D. Vincenzo, C. Cordoni, E. Costa, P. Brunetti, G.B. Bolli, Pharmacokinetics and pharmacodynamics of subcutaneous injection of long-acting human insulin analog glargine, NPH insulin, and ultralente human insulin and continuous subcutaneous infusion of insulin lispro, Diabetes 49 (2000) 2142–2148.
[32] G.A. Brunner, G. Sendhofer, A. Wutte, M. Ellmerer, B. Søgaard, A. Siebenhofer, S. Hirschberger, G.J. Krejs, T.R. Pieber, Pharmacokinetic and pharmacodynamic properties of long-acting insulin analogue NN304 in comparison to NPH insulin in humans, Exp. Clin. Endocrinol. Diabetes 108 (2000) 100–105.
[33] J.L. Whittingham, S. Havelund, I. Jonassen, Crystal structure of a prolonged-acting insulin with albumin-binding properties, Biochemistry 36 (1997) 2826–2831.
[34] S. Havelund, A. Plum, U. Ribel, I. Jonassen, A. Vølund, J. Markussen, P. Kurtzhals, The mechanism of protraction of insulin detemir, a long-acting, acylated analog of human insulin, Pharm. Res. 21 (2004) 1498–1504.